Numerical Study on Flow and Heat Transfer Characteristics Inside Rotating Rib-Roughened Pipe with Axial Throughflow

*WANG Yujie, SUN Wenjing, GAO Qihong, ZHANG Jingzhou**

College of Energy and Power, Nanjing University of Aeronautics and Astronautics, Nanjing 210016, P.R.China

(Received 20 June 2022; revised 10 September 2022; accepted 12 December 2022)

Abstract: A numerical study was performed on the flow and heat transfer characteristics inside a rotating rib-roughened pipe with an axial throughflow, under a fixed axial throughflow Reynolds number Re_x 6 400 and a series of rotational Reynolds number Re_ω ranging from 0 to 3.77×10^4. Three rib configurations were taken into consideration, including ring rib, discrete-ring rib and longitudinal rib, wherein the ring-type ribs were distributed along the axial direction and the longitudinal-type ribs were distributed along the circumferential direction. The results show that the flow field inside a rotating pipe is affected by both axial through flow and rotation-induced azimuthal flow. Under small rotational Reynolds numbers, the axial through flow is dominant such that the ring-type rib plays significant heat transfer enhancement role. Whereas under high rotational Reynolds numbers, the rotation-induced azimuthal flow is dominant such that the longitudinal-type rib is superior to the ring-type rib on heat transfer enhancement. In the view of a comprehensive performance factor that considers both heat transfer enhancement and flow loss together, the discrete-ring rib is identified to be the best among the current three rib configurations under small rotational Reynolds numbers. However, under high rotational Reynolds numbers, the ring-type ribs show no advantage over smooth pipe, and even lead to a reduction in comprehensive performance when compared to the smooth pipe. For the high-speed rotating pipe, the longitudinal-type rib is a promising rib configuration as applied to the heat transfer enhancement.

Key words: rotating pipe; rib configuration; axial throughflow; flow and heat transfer; comprehensive performance factor

CLC number: V231.1 **Document code:** A **Article ID:** 1005-1120(2023)05-0522-12

0 Introduction

The hydrodynamic gas bearing utilizes the gas dynamic pressure compression effect to provide rigid rotor bearing capacity. As it owns some inherent advantages, such as self-acting, no requirements of external pressurization and lubricant supply, and low-cost maintenance, the hydrodynamic gas bearing has been widely applied in the airborne electric-machine system and turbomachineary[1]. To satisfy the technological advancement of airborne electric-machine system and turbomachineary towards more compact size and greater efficiency, the rotational speed needs further prompted such that the thermal effects on the performance of foil journal bearings will significantly behave in the practical applications, due to the strong viscous-shearing inside the thin hydrodynamic gas film[2-4]. Apparently the thermal management becomes one of the quite challenging subjects in the ultra-high speed journal bearings.

Considering that the natural cooling scheme to remove the heat generation inside the hydrodynamic gas film is crucially limited, the use of additional forced cooling is a significant necessity for avoiding impervious degradation and even thermal damage of ultra-high speed journal bearings[5]. During past decades, a lot of efforts were devoted to the thermal management of hydrodynamic foil journal bearings.

*Corresponding author, E-mail address: zhangjz@nuaa.edu.cn.

How to cite this article: WANG Yujie, SUN Wenjing, GAO Qihong, et al. Numerical study on flow and heat transfer characteristics inside rotating rib-roughened pipe with axial throughflow[J]. Transactions of Nanjing University of Aeronautics and Astronautics, 2023, 40(5): 522-533.

http://dx.doi.org/10.16356/j.1005-1120.2023.05.002

Refs.[6-7] proposed two cooling schemes for the radial gas foil bearings, such as the axial throughflow cooling scheme by forcing the cooling air through the film layer axially and air injection cooling scheme by supplying the cooling air into the film layer radially from feeding holes. Ref.[8] proposed a hybrid cooling scheme, wherein two cooling air flow paths were designed, referring as the outer cooling flow that flows through the gas film and foil gap, and the inner cooling flow that flows through the hollow shaft. Ref.[9] performed laboratory tests to identify the aerodynamics of foil bearing under hot surroundings with the use of axial cooling flow. Ref.[10] performed an investigation on the design of the cooling flow passage for the gas foil bearings used in the micro gas turbines. Ref.[11] performed an experimental and theoretical investigation on the thermal behavior of a hybrid bump-metal foil bearing. Different thermal managements with cooling air flows in hollow rotor and bearing substructure were considered and the heat-carrying ratios between two cooling air flows. From aforementioned works, it was exactly sure that the outer cooling flow through the gas film and foil gap played a dominant role on the heat removal of the heat generation inside hydrodynamic gas film. However, the pressure drop inside the outer cooling flow channel was dramatically increased with the increase of operational speed, such that the throughflow capacity was seriously affected in the high-speed operational situations. Therefore, the inner cooling inside a hollow shaft was essential for controlling the temperature rise of rotor.

In the viewing of fundamental flow dynamics, the flow inside a hollow shaft is reasonably modeled as a classical internal flow inside a rotating pipe with an axial throughflow. With respect to the stationary situation, the flow structure inside a rotating pipe is significantly altered by the centrifugal force caused by the rotation, generally leading to a convective heat transfer enhancement but also a stronger pressure drop[12-15]. For the rotating pipes, the installed-rib turbulator is still an effective means for enhancing the convective heat transfer coefficient, following the same principle as that in the stationary pipes[16-18]. To the best of our knowledge, the transverse rib or circular ring-type rib is the main configuration as applied to the stationary pipes, wherein multiple ring-type ribs are distributed along the axial direction to introduce the secondary flow and cause the flow separation and reattachment[19-21]. Discrete ribs have the ability to interrupt the continuous development of the buoyancy layer near the wall, which can reduce the negative effect of buoyancy and enhance heat transfer to a certain extent[22-24]. However, for the circular pipe that rotates about its axis, as the internal flow field is featured by a helicoidal flow structure caused by the superposing of rotation-induced zimuthal movement on the axial through flow, whether the ring-type rib plays the same role on heat transfer enhancement as that in the stationary situation is doubted. In particular, when the rotational speed is high enough the rotation-induced Zimuthal movement is dominate in the internal flow, the flow disturbance role of transverse ribs to the internal helical flow in the rotating situation is conjectured to be changed with respect to the stationary situation. Therefore the rib configuration has significant effects on the internal flow and heat transfer of a rotating pipe with an axial throughflow, which is still lack of deeper identification.

The objective of the present investigation is to assess the effects of rib configuration on the flow and heat transfer inside a rotating rib-roughened pipe with an axial throughflow, by using a numerical methodology. Three rib configurations, including ring-type rib, discrete ring-type rib and longitudinal-type rib, are taken into consideration under a fixed axial-throughflow Reynolds number and a series of rotational Reynolds numbers. From current study, the influences of rotational speed or rotational Reynolds number on the pressure drop and convective heat transfer coefficient are illustrated. In particular, reasonable rib configurations are proposed in accordance with the rotational conditions, in the viewing of the comprehensive performance factor.

1 Physical Model and Simplifications

A typical bump-type hydrodynamic foil journal bearing consists of shaft, foil assembly and bearing sleeve, as schematically shown in Fig.1.

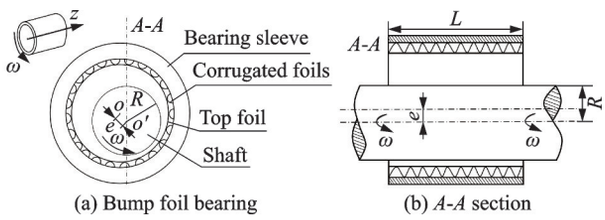

Fig.1 Schematic diagram of hydrodynamic gas bearing structure

During the operation, a self-acting offset of the rotor from the global bearing center is formed, with an eccentricity between the shaft and the bearing sleeve. The hydrodynamic pressure effect of the lubricating gas itself is built up in an eccentric circular gap around the circumference of the bearing, to provide the bearing capacity. Meanwhile, the heat generation inside the hydrodynamic gas film occurs due to the strong viscous heating effect. Considering the current study concerns the internal flow and heat transfer inside a rotating hollow shaft, a researched physical model is taken, as schematically displayed in Fig.2, wherein the supporting section in hydrodynamic foil journal bearing (L=25 mm) is simplified as the heating section by imposing a fixed heat load. In this physical model, the main geometric parameters are denoted as the follows: the radius of shaft R=10.95 mm, the inner diameter of rotating tube d=15 mm, the thickness of tube b=3.45 mm. The front section relative to the heating section has a length of L_e=20 mm and rear section has a length of L_c=45 mm. In order to enhance the heat transfer capacity inside the rotating tube, the rib-roughened turbulators are installed. Three rib configurations are considered, referring as ring-type rib (RT) (Fig.2(a)), discrete ring-type rib (DRT) (Fig.2(b)) and longitudinal-type rib (LT) (Fig.2(c)). Seven rows of ring-type ribs or discrete ring-type ribs are distributed along the axial direction, and twelve longitudinal-type ribs are distributed in the

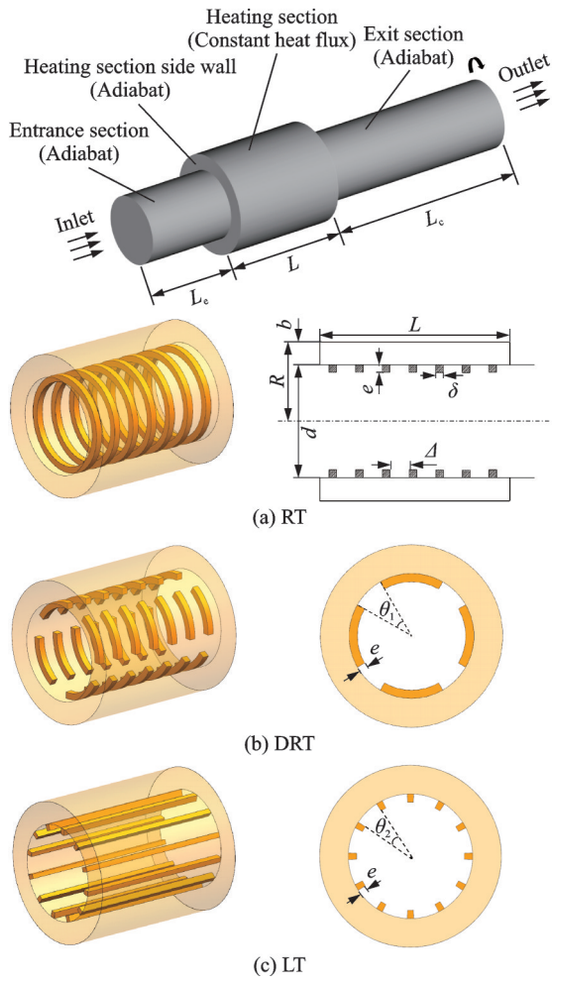

Fig.2 Schematic diagram of rib configurations inside rotating hollow rotor

circumference direction. It has been verified that the rib size is the best comprehensive effect in each rib type. All of the ribs have the same rib height of e=1 mm and rib width of δ=1 m. For the ring-type rib layout, the interval between adjacent ribs is designed as Δ=2.5 mm. For the discrete ring-type rib layout, the intersection angle corresponding to the circumference interval is designed as θ_1=30°. For the longitudinal-type rib layout, the intersection angle between adjacent ribs is designed as θ_2=24°.

2 Description of Computational Methodology

2.1 Numerical modeling

Considering the internal flow in a pipe that rotates about its axis with a rotating angular velocity ω, the governing equations for momentum and ener-

gy transports are modified in the relative velocity or rotating reference frame, wherein the relative velocity is used[25]

$$\nabla\cdot\rho\boldsymbol{v}_r=0 \tag{1}$$

$$\nabla\cdot\left(\rho\boldsymbol{v}_r\boldsymbol{v}_r\right)+\rho(2\boldsymbol{\omega}\times\boldsymbol{v}_r+\boldsymbol{\omega}\times\boldsymbol{\omega}\times r)=-\nabla p+\nabla\cdot\boldsymbol{\tau}+\boldsymbol{F} \tag{2}$$

$$\nabla\cdot\left(\rho v_r H_r\right)=\nabla\cdot(k\nabla T+\boldsymbol{\tau}\cdot\boldsymbol{v}_r) \tag{3}$$

where $\boldsymbol{v}_r$ is the relative velocity and $\boldsymbol{\tau}$ the viscous stress. The momentum equation contains two additional terms, the Coriolis acceleration term ($2\boldsymbol{\omega}\times\boldsymbol{v}_r$) and the centripetal acceleration term ($\boldsymbol{\omega}\times\boldsymbol{\omega}\times r$). Since local temperature changes and local pressure changes will cause density changes, resulting in buoyancy, the centrifugal buoyancy term $\boldsymbol{F}=\rho_0\beta\Delta T(\boldsymbol{\omega}\times\boldsymbol{\omega}\times r)$ is introduced, and ρ_0 is the reference density. The energy equation uses the relative total enthalpy H_r and ($\boldsymbol{\tau}\cdot\boldsymbol{v}_r$) is the energy transport due to viscous dissipation. ρ and k are the density and thermal conductivity of air, respectively.

The corresponding boundary conditions are summarized as the follows:

(1) For the rotating pipe, a rotating angular velocity ω is given, and the rotational Reynolds number Re_ω is defined as

$$Re_\omega=\frac{\rho\omega d^2}{4\mu} \tag{4}$$

where μ is the dynamic viscosity of air.

(2) The inlet of axial throughflow is set as velocity inlet by giving the mass flowrate Q_m. The inlet temperature is set as 300 K. The axial throughflow inlet Reynolds number Re_x is defined as

$$Re_x=\frac{\rho U_{in}d}{\mu} \tag{5}$$

where U_{in} is the bulk-averaged velocity at tube inlet.

(3) The outlet is set as a pressure out, by setting $p_{out}=101\ 325$ Pa.

(4) On the heating section, a constant heat flux q is imposed. Whereas for the other solid surface, the adiabatic thermal condition is adopted. On the solid surface, no slip velocity is adopted.

In the current study, the mass flowrate of axial throughflow is set as $Q_m=5$ kg/h and the corresponding axial-throughflow inlet Reynolds number Re_x is about 6 400. The rotating angular velocity ω is varied between 0 r/min and 1×10^5 r/min, and the corresponding rotational Reynolds number Re_ω is varied from 0 to 3.77×10^4. The heat flow of the rotor surface under different conditions is obtained by numerical calculation, and the average value is selected as the thermal boundary condition of this study. The heat flux imposing on the heating section is set as $q=6\ 950$ W/m^2. During the fluid-solid coupling, the thermal conductivity of solid wall is set as 16.3 W/(m·K).

2.2 Computational methodology

The current numerical simulations are performed by using the commercial CFD solver ANSYS Fluent, wherein 3-D steady-state flow and temperature fields are solved. The working fluid is treated as an ideal gas on account of the compressible effect. Its thermal physical parameters are set as the ideal-gas based density. Kinetic-theory based specific heat and thermal conductivity. Sutherland law based viscosity. The second order upwind scheme is used for the spatial discretization of convective terms in the conservation equations. In the momentum equation, the PRESTO scheme is used for the discretization of pressure gradient term. With regard to the pressure-velocity coupling, the SIMPLE algorithm is adopted. The convergence is regarded to be achieved when all normalized residuals of concerned variables fell below 1.0×10^{-5}.

Computational grids are generated by using ICEM software. The structured meshes are adopted in the whole computational domain. The first layer of computational meshes is located at near-wall zone with a space of 0.02 mm normally to the solid surface, and y^+ is 1, which meets the requirement of the enhanced wall function. Then the computational meshes are stretched away from the viscous wall using a stretching ratio of 1.1. To make sure the computational result is independence of the computational mesh, a grid independency test is carried out in advance. As demonstrated in Fig.3 (l/D is the ratio of the length between the position on the heating section and the inlet to the diameter of the channel), when the grid number is beyond 2.9 million the computed circumference-averaged temperature

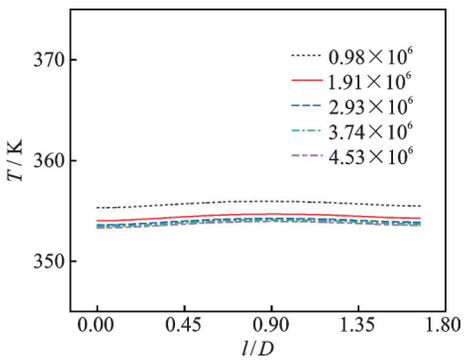

Fig.3 Grid independence test

distribution at the heating section is not sensitive to the grid number. Thus a final grid number is selected around 3 million.

To justify the current computational methodology on modelling the flow field inside a rotating pipe, an example validation is performed in advance against the experimental test by Imao et al[12]. Beside, the selection of reasonable two-equation turbulence model for the the turbulence closure is also made from the comparison. As demonstrated in Fig.4 (r/R is the ratio of the radial position to the radius of the pipe), it is confirmed that all the selected two-equation turbulence models provide nearly the same prediction on the azimuthal velocity profile in

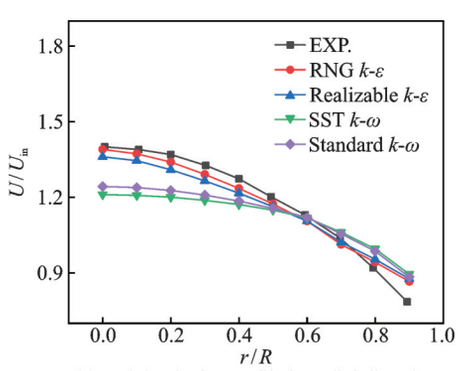

(a) Axial velocity profile in radial direction

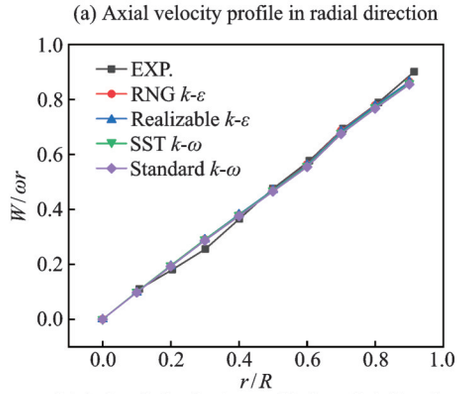

(b) Azimuthal velocity profile in radial direction

Fig.4 Validation of turbulence models

radial direction, and $W/\omega r$ is the ratio of the tangential velocity to the tangential velocity of the rotating pipe. Regarding the axial velocity profile in radial direction (U/U_{in} is the ratio of the axial velocity to the inlet velocity), it is found both RNG k-ε turbulence model and Realizable k-ε turbulence model could provide more correct prediction with respect to the experimental data. Referring previous researches relating to the numerical simulations of rotating flow[26-28], RNG k-ε turbulence model is selected in current study.

3 Results and Discussion

3.1 Flow fields

In a rotating tube, the Coriolis force and centrifugal force caused by the rotation make the internal flow complicated when compared to the stationary situation. Fig.5 shows the local three-dimensional flow trajectories inside a smooth pipe (SP), colored by the temperature value. Generally, the flow field inside a rotating pipe suffers to dual roles of forced axial through flow and rotation-induced azimuthal flow. When the pipe rotates at a small rotating speed or rotational Reynolds number (such as $Re_\omega = 807$), the azimuthal flow induced by pipe rotation makes the flow trajectory deflect slightly in the circumferential direction. At a big radial location where the local flow zone is close to the rotating wall, the flow trajectory deflection behaves more strongly because of radially growing centrifugal forces. In a total, the forced axial through flow is dominant in the situations of small rotating speeds. However, when the pipe rotates at a high rotating speed or rotational Reynolds number (such as $Re_\omega = 3.77\times10^4$), the rotation-induced azimuthal flow is dominate on the internal flow field, making the flow trajectories take on a significant spiral flow feature, because of the superposing of axial through flow. When compared to the small rotational Reynolds number situation, the axial flow in the entrance section is concentrated to the central zone of the rotating pipe, indicating that the inlet flow of forced axial flow is locally blocked at the big radial location because of the rotation effect. Along the axial direc-

tion, the spiral flow trajectory extends outward in the radial direction gradually. Meanwhile, the fluid temperature in the near-wall zone of heating section is obviously higher than that in the small rotational Reynolds number situation, indicating that the convective heat transfer capacity is raised in the high rotational Reynolds number situation.

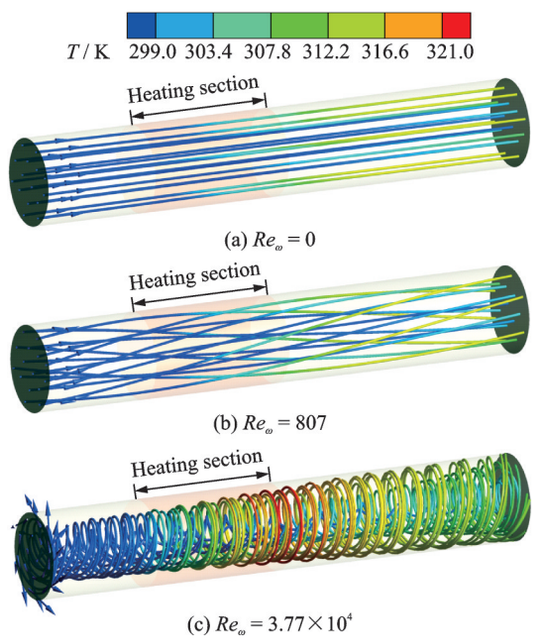

Fig.5 Flow trajectories inside smooth pipe under stationary and rotating states

The rotation-induced azimuthal flow changes the static pressure distribution inside the pipe, as demonstrated in Fig.6. In the stationary situation, the internal flow along the flow direction is classically characterized by a relatively regular favourable-pressure flow. With the increase of rotational Reynolds number, the static pressure in the near-wall zone is increased because the near-wall fluid suffers the stronger Coriolis force and centrifugal force. Meanwhile, the static pressure in the central zone of a rotating pipe is decreased on the otherwise. Especially, when the pipe rotates at a high rotational Reynolds number, a low-pressure zone occurs inside the rotating pipe, occupying nearly entire axial length. This formation of low-pressure zone not only affects the internal flow inside the pipe, but also affects the outflow at the outlet. Due to this low-pressure zone, the external ambient air would even be suctioned into the central zone of a rotating pipe

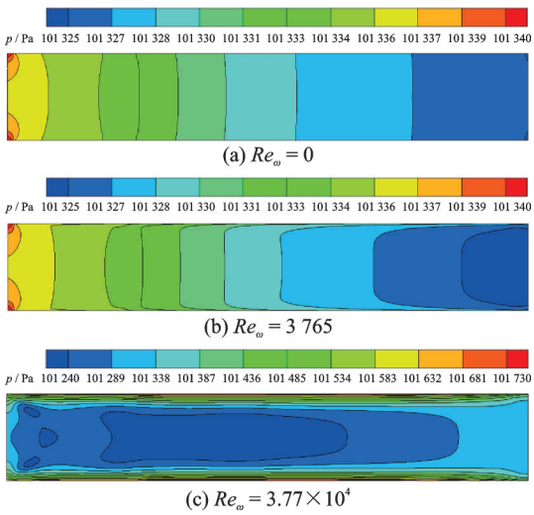

Fig.6 Pressure contours in side smooth pipe

from the outlet plane.

As the internal flow field is dramatically changed by the rotational effect, the roles of rib-roughened turbulators on the flow disturbance are conjectured to be changed in accordance with the rotational Reynolds number. The local streamlines in the vicinity of rib-roughened zone are displayed in Figs.7—9, corresponding to different rib configurations. In these figures, the streamlines are colored by the dimensionless velocity, or the velocity ratio of locally absolute velocity to the bulk-averaged velocity at tube inlet (U_{in}).

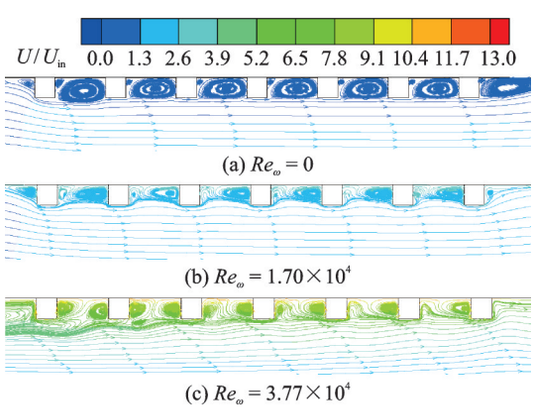

Fig.7 Local streamlines inside RT

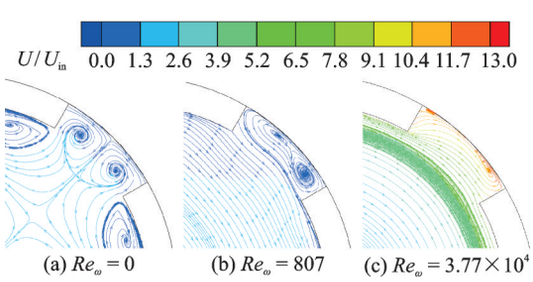

Fig.8 Local streamlines inside DRT

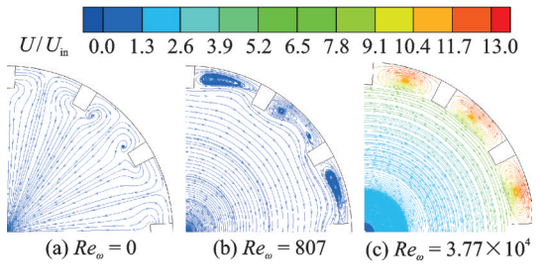

Fig.9 Local streamlines inside LT

For the RT, a large-scale vortex structure is formed in the interval region after the axial through flow passes through the ribs in the stationary situation, as displayed in Fig.7(a). The transverse rib plays a promising flow disturbance role on the internal flow. As the rotational Reynolds number increases, the flow velocity in the high radial location is increased. The rotation-induced azimuthal flow becomes dominate gradually, making the size of vortex structure between ribs reduction radially, as displayed in Fig.7(b). In particular, under a high rotational Reynolds number, the rotation-induced azimuthal flow is dominant significantly, the absolute velocity near the wall surface is obviously greater than the bulk-averaged velocity of the axial throughflow, the flow disturbance role of ring-type rib on the helicoidal flow is apparently weakened with respective to the stationary situation, as demonstrated in Fig.7(c). Also, it is conjectured that the heat transfer enhancement role of ring-type rib layout would be reduced in the high rotational Reynolds number situation.

For the DRT, the flow disturbance role on the internal flow is nearly the same as the ring-type rib layout. Because there is a gap between discrete ring ribs in the circumferential direction, the local flow disturbance also appears in the vicinity of this gap in the stationary situation, as displayed in Fig.8(a). In the rotating situations, the discrete ring ribs could introduce a flow disturbance role to the rotation-induced azimuthal flow, as displayed in Fig.8(b) and Fig.8(c).

For the LT, the flow disturbance role of longitudinal rib on the axial flow is very weak in the stationary situation, as displayed in Fig.9(a). However, in the rotating situations, the longitudinal rib layout shows its superiority on disturbing the local flow in the rib-roughened region, to the rotation-induced azimuthal flow. Under a small rotational Reynolds number, the rotation-induced azimuthal velocity is small, such that the vortex structure is composed by the low-velocity fluid, as displayed in Fig.9(b). Under a high rotational Reynolds number, the rotation-induced azimuthal velocity is strong, such that the vortex structure is composed by the high-velocity fluid, as displayed in Fig.9(c).

From the above-mentioned analysis, it is confirmed that the rotation has a significant effect on the internal flow field, altering the flow disturbance roles of rib layout on the internal flow. As a consequence, the heat transfer enhancement role of rib layout would be changed in accordance with the rotational Reynolds number.

3.2 Flow and heat transfer performances

Fig.10 displays the temperature contours in the solid region at the middle plane of heating section, in the stationary situation. It is seen that temperature of heating section could be effectively reduced by utilizing the inner rib-roughened configurations, when compared to the SP at the same axial throughflow mass flow rate. By comparing three different rib configurations, the ring-type ribs, either in continuous (RT) or discrete (DRT), provide better cooling roles than the LT. With respect to the SP, the RT could reduce the peak temperature of heating section about 64K. Only about 34 K reduction is

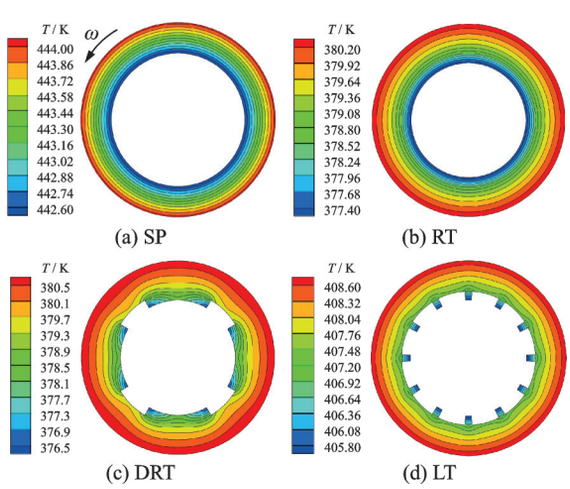

Fig.10 Temperature contours on middle-axial plane of heating section under $Re_\omega = 0$

achieved by the LT.

Fig.11 displays the temperature contours in the solid region at the middle plane of heating section, in the rotating situation at $Re_\omega = 3.77\times10^4$. When compared to the stationary situation, the peak temperature is reduced obviously because the strong helicoidal flow enhances the convective heat transfer capacity. Taking the SP as an example, the peak temperature is reduced about 70 K in the high rotational Reynolds number situation relative to the stationary situation. With respect to the SP, the rotation effect on internal convective heat transfer of rib-roughened tube is weakened. In particular, for the RT, the peak temperature under $Re_\omega = 3.77\times10^4$ has only about 16 K reduction in relative to the stationary situation. When compared to the SP at the same rotational Reynolds number, only about 9 K reduction in the peak temperature is achieved by the RT. Apparently, in the high rotational Reynolds number situation, the LT presents the best convective heat transfer enhancement owing to its strongest flow disturbance role to the rotation-induced azimuthal flow.

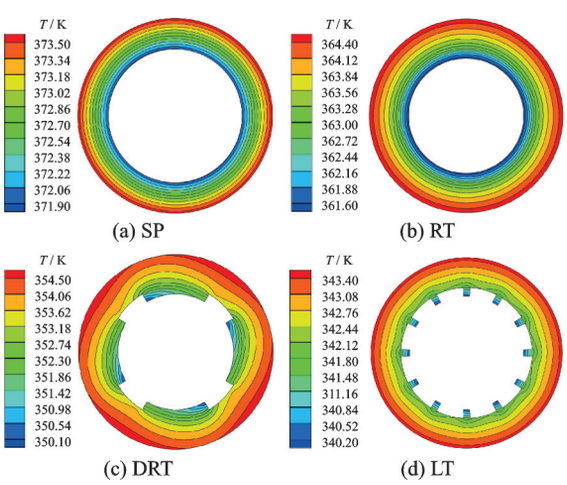

Fig.11 Temperature contours on middle-axial plane of heating section under $Re_\omega = 3.77\times10^4$

Fig.12 displays the peak temperature variations of heating section with the rotational Reynolds number. It is seen that the peak temperature is decreased with the increase of rotational Reynolds number generally. For the SP and LT, the peak temperature is reduced rapidly with the rotational Reynolds number when Re_ω is increased from 0 to 1×10^4. While for the RT and DRT, the peak temperature is not sensitive to the rotational Reynolds number in a wide range. It is noteworthy that when the rotational Reynolds number is less than 2 400, the RT and DRT provide a better heat transfer enhancement than the LT. Whereas under high rotational Reynolds numbers, the LT is more pronounced for reducing the peak temperature of heating section.

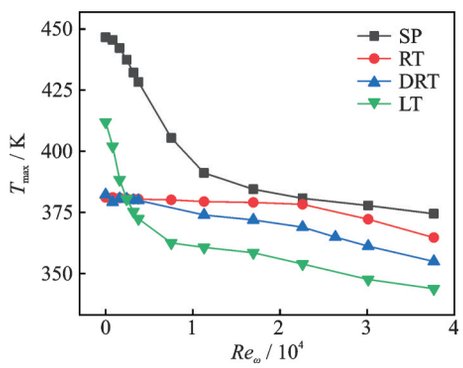

Fig.12 Effects of rotational Reynolds number and rib type on peak temperature of rotor

The rib-roughened configuration inside a rotating tube enhances the convective heat transfer but also leads to a serious pressure loss. In order to assess the comprehensive effects of ribbed configuration, a comprehensive performance factor is introduced, which is defined as

$$\mathrm{PEC} = \frac{\overline{Nu}/Nu_0}{(f/f_0)^{1/3}} \tag{6}$$

where Nu is the area-averaged Nusselt number and f the friction factor. The subscript "0" represents the baseline case for the comparison. Here the corresponding smooth tube under the same rotational Reynolds number is selected as baseline case.

The area-averaged Nusselt number over the heating section and the friction factor across the entire pipe are defined as

$$\overline{Nu} = \frac{hd}{\lambda} \tag{7}$$

$$f = \frac{2(p_{in} - p_{out})}{\rho U_{in}^2 L/d} \tag{8}$$

where h is the area-averaged convective heat transfer coefficient over the inner surface of heating section; λ and ρ are the thermal conductivity and the density of the air, respectively; $(p_{in}-p_{out})$ is the

pressure drop of the internal flow across the length L of the pipe.

For the SP, the effects of rotation on the area-averaged Nusselt number Nu_0 and friction factor f_0 are displayed in Fig.13. In general, both the convective heat transfer and the flow loss are increased monotonically with the rotational Reynolds number. However, the influencing tendency of rotational Reynolds number on Nu_0 is somewhat different from that on f_0. Regarding the convective heat transfer capacity, as seen in Fig.13(a), Nu_0 is increased rapidly along the rotational Reynolds number in a nearly linear mode when Re_ω is increased from 0 to 1×10^4. When Re_ω is beyond 1×10^4, the increase rate of Nu_0 along Re_ω becomes degraded. Whereas regarding the friction factor, as seen in Fig.13(b), f_0 is weakly increased along the rotational Reynolds number when Re_ω is less than 0 to 1×10^4. When Re_ω is beyond 2×10^4, the friction factor is increased sharply with the rotational Reynolds number. Identified from Fig.13, under a high rotational Reynolds number of $Re_\omega=3.77\times10^4$, the Nusselt number and friction factor are about two times and five times of the corresponding values in the stationary situation, respectively.

Fig.14 shows the variations of average Nusselt number $\overline{Nu}$ and friction factor f with the rotational Reynolds number, for the rib-roughened pipes. It is confirmed that the effects of rotation on the Nusselt number and friction factor of rib-roughened pipe are similar to the smooth pipe. However, the variation tendencies of convective heat transfer and friction with rotational Reynolds number are somewhat distinct for different rib-roughened configurations, because of different flow disturbance roles of rib layout on the internal flow. Taking the SP as a baseline case for comparison, Fig.15 presents directly the variation patterns of convective heat transfer enhancement ratio ($\overline{Nu}/Nu_0$), friction factor ratio (f/f_0) and comprehensive performance factor (PEC) along with the the rotational Reynolds number, for three different rib-roughened configurations. With respect to the baseline SP, all the rib-roughened pipes show their heat transfer enhancement role but also increase the flow loss. Their influencing roles are tightly dependent on the rotational

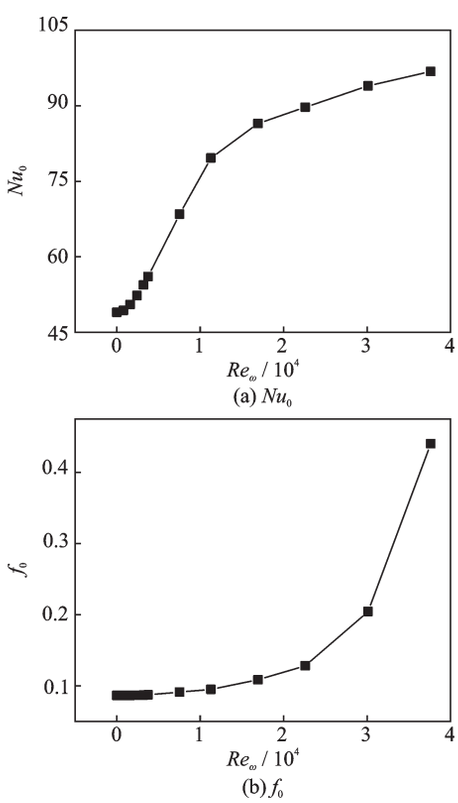

Fig.13 Effects of rotational Reynolds number on Nu_0 and f_0 for smooth pipe

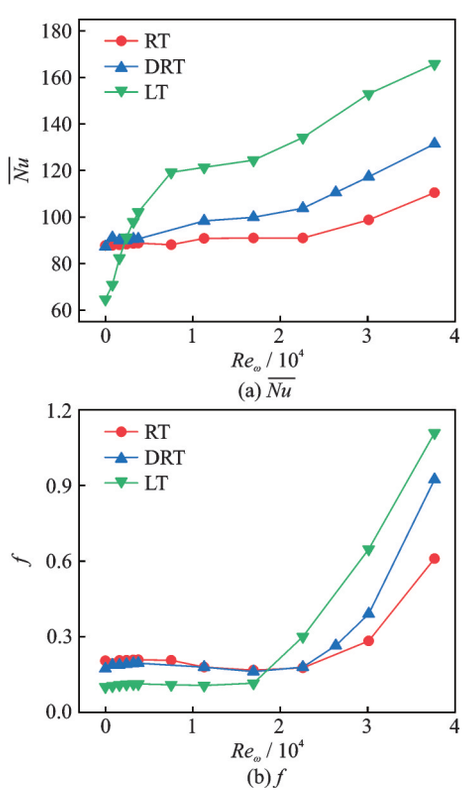

Fig.14 Effects of rotational Reynolds number on $\overline{Nu}$ and f for rib-roughened pipes

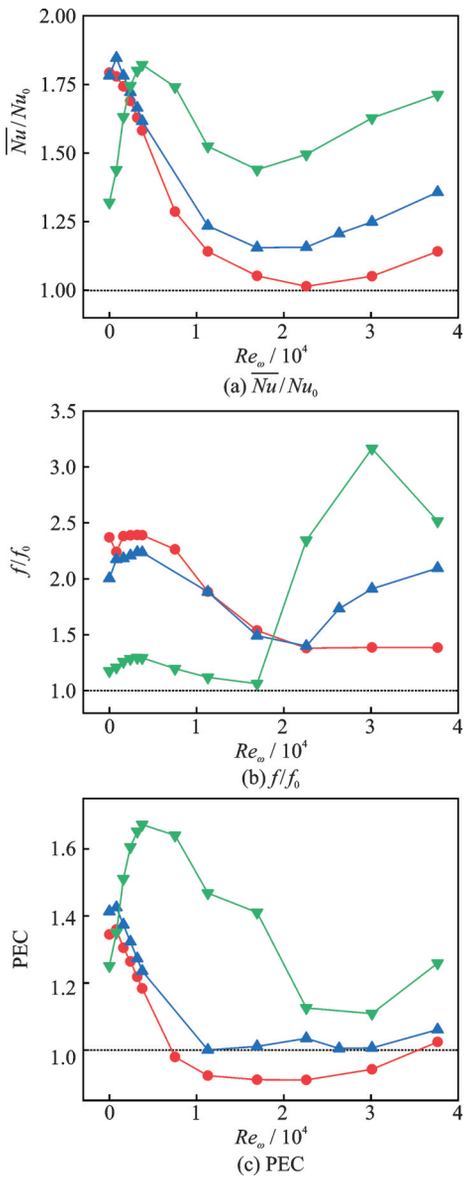

Fig.15 Comparison between different rib configurations in view of comprehensive factor

Reynolds number, showing a non-monotonic variation.

Under small rotational Reynolds numbers (such as $Re_\omega < 2\,400$), the RT and DRT provide bigger convective heat transfer enhancement ratio but also bigger friction factor ratio than the LT. In the viewing of the comprehensive performance factor that considers both heat transfer enhancement and flow loss together, the DRT is identified to be the best among the current three rib configurations.

Under high rotational Reynolds numbers (such as $Re_\omega > 2\times10^4$), the LT provide bigger convective heat transfer enhancement ratio but also bigger friction factor ratio than the RT. It is noteworthy the RT show no advantage over SP, and even lead to a reduction in the comprehensive performance factor when compared to the smooth pipe. Therefore, for the high-speed rotating tube, the LT is suggested to be a more promising rib configuration as applied to the heat transfer enhancement.

4 Conclusions

A numerical study is conducted to illustrate the flow and heat transfer characteristics inside a rotating rib-roughened pipe with an axial throughflow, under a fixed axial-throughflow Reynolds number Re_x of 6 400 and a series of rotational Reynolds number Re_ω ranging from 0 to 3.77×10^4. Three rib configurations, including RT, DRT and LT, are taken into consideration. From current study, the main conclusions are summarized as the follows:

(1) The flow field inside a rotating pipe is of high complexity, due to the dual influencing aspects from the axial through flow and the rotation-induced azimuthal flow. The dominant flow feature and subsequently the flow of rib-roughened flow disturbance role is tightly dependent on the competition between axial through flow and rotation-induced azimuthal flow.

(2) Under small rotational Reynolds numbers, the axial through flow is dominant such that the RT plays a significant flow disturbance role and subsequently the strong heat transfer enhancement. Whereas under high rotational Reynolds numbers, the rotation-induced azimuthal flow is dominant such that the LT is superior to the RT on the flow disturbance and subsequently heat transfer enhancement.

(3) Evaluated on the comprehensive performance factor that considers both heat transfer enhancement and flow loss together, the DRT is identified to be the best among the current three rib configurations under small rotational Reynolds numbers. However, under high rotational Reynolds numbers, the LT layout is a promising rib configuration as applied to the heat transfer enhancement.

References

[1] SAMANTA P, MURMU N C, KHONSARI M M.

The evolution of foil bearing technology[J]. Tribology International, 2019, 135: 305-323.

[2] KIM T H, BREEDLOVE A W, SAN ANDRES L. Characterization of a foil bearing structure at increasing temperatures: Static load and dynamic force performance [J]. ASME Journal of Tribology, 2009, 131: 041703.

[3] RYU K, SAN ANDRES L. On the failure of a gas foil bearing: High temperature operation without cooling flow[J]. Journal of Engineering Gas Turbines and Power, 2013, 35: 112506.

[4] SIM K, LEE Y B, SONG J W, et al. Identification of the dynamic performance of a gas foil journal bearing operating at high temperatures[J]. Journal of Mechanical Science and Technology, 2014, 28: 43-51.

[5] SALEHI M, SWANSON E, HESHMAT H. Thermal features of compliant foil bearings-theory and experiments[J]. ASME Journal of Tribology, 2001, 123: 566-571.

[6] RADIL K, DELLACORTE C, ZESZOTEK M. Thermal management techniques for oil-free turbomachinery systems[J]. Tribology Transactions, 2008, 50 (3): 319-327.

[7] RADIL K, BATCHO Z. Air injection as a thermal management technique for radial foil air bearings[J]. Tribology Transactions, 2011, 54(4): 666-673.

[8] KIM T H, SAN ANDRES L. Thermohydrodynamic model predictions and performance measurements of bump-type foil bearing for oil-free turboshaft engines in rotorcraft propulsion systems[J]. ASME Journal of Tribology, 2010, 132: 011701.

[9] RYU K. Prediction of axial and circumferential flow conditions in a high temperature foil bearing with axial cooling flow[J]. Journal of Engineering Gas Turbines and Power, 2012, 134: 094503.

[10] LEE D H, LIM H S, CHOI B S, et al. Thermal behavior of radial foil bearings supporting on an oil-free gas turbine: Design of the cooling flow passage and modeling of the thermal system[J]. Journal of Engineering Gas Turbines and Power, 2017, 139: 061902.

[11] ZHANG K, ZHAO X Y, FENG K, et al. Thermohydrodynamic analysis and thermal management of hybrid bump-metal mesh foil bearings: Experimental tests and theoretical predictions[J]. International Journal of Thermal Sciences, 2018, 127: 91-104.

[12] IMAO S, ITOH M, HARADA T. Turbulent characteristics of the flow in an axially rotating pipe[J]. International Journal of Heat and Fluid Flow, 1996, 17 (5): 444-451.

[13] SEGHIR-OUALI S, SAURY D, HARMAND S, et al. Convective heat transfer inside a rotating cylinder with an axial airflow[J]. International Journal of Thermal Sciences, 2006, 45(12): 1166-1178.

[14] OULD-ROUISS M, DRIES A, MAZOUZ A. Numerical predictions of turbulent heat transfer for airflow in rotating pipe[J]. International Journal of Heat and Fluid Flow, 2010, 31(4): 507-517.

[15] SHAME B. Thermally developing turbulent flow and heat transfer in an axially rotating pipe[J]. International Journal of Fluid Mechanics Research, 2020, 47 (6): 573-582.

[16] NOBARI M R H, GHARALI K. A numerical study of flow and heat transfer in internally finned rotating straight pipes and stationary curved pipes[J]. International Journal of Heat and Mass Transfer, 2006, 49: 1185-1194.

[17] YASSIN M A, SHEDID M H, ABD El-HAMEED H M, et al. Heat transfer augmentation for annular flow due to rotational of inner finned pipe[J]. International Journal of Thermal Sciences, 2018, 134: 653-660.

[18] ABOTSI O Y W, KIZITO J P. Numerical study of heat transfer in an axially rotating pipe equipped with Kenics mixer[J]. Case Studies in Thermal Engineering, 2020, 21: 100695.

[19] KIML R, MAGDA A, MOCHIZUKI S, et al. Rib-induced secondary flow effects on local circumferential heat transfer distribution inside a circular rib-roughened tube[J]. International Journal of Heat and Mass Transfer, 2004, 47: 1403-1412.

[20] KIM K M, KIM B S, LEE D H, et al. Optimal design of transverse ribs in tubes for thermal performance enhancement[J]. Energy, 2010, 35: 2400-2406.

[21] HUANG W C, CHEN C A, SHEN C, et al. Effects of characteristic parameters on heat transfer enhancement of repeated ring-type ribs in circular tubes[J]. Experimental Thermal and Fluid Science, 2015, 68: 371-380.

[22] YUAN N, BI D P, ZHAI Y L, et al. Flow and heat transfer performance of supercritical pressure carbon dioxide in pipes with discrete double inclined ribs[J]. International Journal of Heat and Mass Transfer, 2020, 149:119175.

[23] AZAD R, BHUVAD S, LANJEWAR A. Study of solar air heater with discrete arc ribs geometry: Experimental and numerical approach[J]. International Journal of Thermal Sciences, 2021,167: 107013.

[24] WANG J S, LIU J, WANG L, et al. Numerical in-

vestigation of heat transfer and fluid flow in a rotating rectangular channel with variously-shaped discrete ribs[J]. Applied Thermal Engineering, 2018, 129: 1369-1381.

[25] GAO Q H, ZHANG J Z, TAN X M. Numerical study on pressure drop and temperature rise of an axial throughflow passing through rotating cavity[J]. Journal of Propulsion Technology, 2021, 42(9): 2062-2070.

[26] OWEN J M, ABRAHAMSSON H, LINDBLAD K. Buoyancy-induced flow in open rotating cavities[J]. Journal of Engineering Gas Turbines and Power, 2007, 129: 893-900.

[27] NOURI-BORUJERDI A, NAKHCHI M E. Prediction of local shear stress and heat transfer between internal rotating cylinder and longitudinal cavities on stationary cylinder with various shapes[J]. International Journal of Thermal Sciences, 2019, 138: 512-520.

[28] MURTHY S D S. Analysis and optimization of thermal characteristics in a rotating packed bed[J]. Applied Thermal Engineering, 2020, 165: 114533.

Authors Ms. **WANG Yujie** received her B.S. degree in engineering from Nanjing Normal University in 2020, and is now studying at Nanjing University of Aeronautics and Astronautics(NUAA). Her research is focused on heat transfer enhancement technology.

Prof. **ZHANG Jingzhou** received his B.S. degree in engineering from Tsinghua University in 1986 and Ph.D. degree in engineering from NUAA in 1992. He joined in NUAA in 1992. His research is focused on heat transfer enhancement technology and infrared stealth technology.

Author contributions Ms. **WANG Yujie** proposed the research topic, completed the research plan design, numerical simulation, result processing and other processes, and wrote the manuscript of the paper. Dr. **SUN Wenjing** provided assistance in literature organization and data analysis. Mr. **GAO Qihong** contributed to the discussion and background of this study. Prof. **ZHANG Jingzhou** carried out the overall planning and content control of the whole research process, and put forward many constructive comments on the revision and improvement of the manuscript. All authors commended on the manuscript draft and approved the submission.

Competing interests The authors declare no competing interests.

(Production Editor: SUN Jing)

带轴向通流旋转管内部肋结构的流动传热特性数值研究

王宇婕，孙文静，高齐宏，张靖周

(南京航空航天大学能源与动力学院，南京 210016，中国)

摘要：采用数值模拟方法，在轴向通流雷诺数Re_x为6 400、旋转雷诺数Re_ω变化范围为0～3.77×10^4的条件下，对带轴向通流旋转管内部肋结构的流动传热特性进行了研究，着重研究了3种肋型结构，包括沿轴向布置的环形横肋、离散环肋和沿周向布置的纵向直肋。研究结果表明，旋转通道内流场受到轴向通流流动和旋转诱导周向流动的共同影响，在低旋转雷诺数下，轴向通流流动占主导，环肋和离散环肋的传热强化机制显著；而在高的旋转雷诺数下纵向肋的传热强化机制则更为显著。采用综合性能因子对几种肋型进行综合评价，在低旋转雷诺数下离散环肋的综合性能最优，但在高旋转雷诺数下，环肋和离散环肋结构的综合性能相较于光滑通道并无优势，甚至还会导致综合性能的降低。对于高速旋转管，纵向肋是内部强化传热应用的一种合理结构形式。

关键词：旋转管；肋结构；轴向通流；流动传热；综合性能因子